PAPER

Spencer–Attix water/medium stopping-power ratios for the dosimetry of proton pencil beams

Phys. Med. Biol. **58** (2013) 2509–2522 doi:10.1088/0031-9155/58/8/2509

Spencer–Attix water/medium stopping-power ratios for the dosimetry of proton pencil beams

C Gomà[1,2], P Andreo[3] and J Sempau[4]

[1] Centre for Proton Therapy, Paul Scherrer Institute, Villigen PSI, Switzerland
[2] Department of Physics, Swiss Federal Institute of Technology Zurich, Zurich, Switzerland
[3] Medical Radiation Physics, Stockholm University at Karolinska University Hospital, Stockholm, Sweden
[4] Institut de Tècniques Energètiques, Universitat Politècnica de Catalunya, Barcelona, Spain

E-mail: carles.goma@psi.ch

Received 3 December 2012, in final form 13 February 2013
Published 21 March 2013
Online at stacks.iop.org/PMB/58/2509

Abstract

This paper uses Monte Carlo simulations to calculate the Spencer–Attix water/medium stopping-power ratios ($s_{w,med}$) for the dosimetry of scanned proton pencil beams. It includes proton energies from 30 to 350 MeV and typical detection materials such as air (ionization chambers), radiochromic film, gadolinium oxysulfide (scintillating screens), silicon and lithium fluoride. Track-ends and particles heavier than protons were found to have a negligible effect on the water/air stopping-power ratios ($s_{w,air}$), whereas the mean excitation energy values were found to carry the largest source of uncertainty. The initial energy spread of the beam was found to have a minor influence on the $s_{w,air}$ values in depth. The water/medium stopping-power ratios as a function of depth in water were found to be quite constant for air and radiochromic film—within 2.5%. Also, the $s_{w,med}$ values were found to have no clinically relevant dependence on the radial distance—except for the case of gadolinium oxysulfide and proton radiography beams. In conclusion, the most suitable detection materials for depth-dose measurements in water were found to be air and radiochromic film active layer, although a small correction is still needed to compensate for the different $s_{w,med}$ values between the plateau and the Bragg peak region. Also, all the detection materials studied in this work—except for gadolinium oxysulfide—were found to be suitable for lateral dose profiles and field-specific dose distribution measurements in water.

(Some figures may appear in colour only in the online journal)

1. Introduction

The commissioning of scanned proton pencil beams requires (i) reference dose measurements to calibrate the beam monitor chambers, (ii) relative dose measurements—depth-dose curves

and lateral dose profiles—to feed the treatment planning system (TPS), and (iii) field-specific dose distribution measurements to validate the dose distribution predicted by the TPS.

According to IAEA TRS-398 (Andreo *et al* 2000), the absorbed dose to water (D_w) under reference conditions should be measured in water with a cylindrical or plane-parallel ionization chamber. Depth-dose curves should also be measured in water (Andreo *et al* 2000) with a large-diameter plane-parallel ionization chamber (ICRU 2007). Lateral dose profiles are typically measured with high spatial resolution detectors—such as radiochromic films (Gillin *et al* 2010) or scintillating screens coupled to a CCD camera[5] (Pedroni *et al* 2005)—or with small volume ionization chambers such as a pin-point chamber (Gillin *et al* 2010, Schwaab *et al* 2011). Finally, field-specific dose distributions are typically measured with two-dimensional detectors such as ionization chamber matrices (Karger *et al* 2010), radiochromic films (Albertini *et al* 2011) or scintillating screens (Boon *et al* 2000).

All these measurements—performed with different detectors and detection materials—will most likely be converted to absorbed dose to water. To correctly perform this step, it is essential to know the water/medium stopping-power ratio ($s_{w,med}$) of the detection material and the perturbation factor (p) of the detector. In this paper, we address the calculation of $s_{w,med}$—which is a property of the detection material and the radiation field. The calculation of the perturbation factor—which is a property of the detector and the radiation field—is beyond the scope of this work and it will not be addressed here.

In the field of proton therapy, the largest contributions to the calculation of stopping-power ratios have historically focused on the water/air stopping-power ratio ($s_{w,air}$)—because of its importance for reference dosimetry. Medin and Andreo (1997) calculated the $s_{w,air}$ values for monoenergetic proton beams from 50 to 250 MeV with their self-developed Monte Carlo code PETRA—where nuclear inelastic processes were take into account but only protons (both primary and secondary) and delta-ray electrons were tracked. They found delta-ray electrons should be included in the calculation of $s_{w,air}$ whereas alpha particles could be omitted. Later, Laitano and Rosetti (2000) calculated the $s_{w,air}$ values for proton beams with a realistic energy spectra—with FLUKA (Ferrari *et al* 2005)—and they found no significant differences with the $s_{w,air}$ values obtained for monoenergetic beams. Finally, Andreo *et al* (2000) derived the $s_{w,air}$ values for passively-scattered proton beams.

Based on these past results, the aim of this work is to use Monte Carlo simulations:

(i) To calculate the $s_{w,med}$ values for the detection materials most commonly used in the dosimetry of proton pencil beams. These detection materials are: air (ionization chambers), radiochromic film (Gafchromic® EBT2/EBT3 active layer[6]) and gadolinium oxysulfide (Gd_2O_2S:Tb, a scintillating material). Silicon (Si) and lithium fluoride (LiF) were also included for completeness. Special attention was paid to $s_{w,air}$ because of its importance in reference dosimetry.

(ii) To extend the energy range from 30 to 350 MeV, to take into account the upcoming generation of proton therapy beam delivery systems.

(iii) To investigate the influence of particles heavier than protons and track-ends on the calculation of the stopping-power ratios.

(iv) To investigate the effect of the initial energy spread of the beam on the stopping-power ratios.

[5] In what follows, and for the sake of simplicity, we will refer to this kind of detectors as scintillating screens.

[6] According to the manufacturer (Ashland 2011), the active layers of EBT2 and EBT3 films are identical. In what follows, and for the sake of simplicity, we will refer to the EBT2/EBT3 active layer by simply EBT2.

(v) To investigate the dependence of $s_{w,med}$ on the radial distance (perpendicular to the beam direction). This last point was inspired by the results of Grassberger and Paganetti (2011) showing an increased LET in the penumbra region of clinical proton beams.

2. Materials and methods

The $s_{w,med}$ values were obtained by means of the Spencer–Attix cavity theory (Nahum 1978). For multiple charged particles, the $s_{w,med}$ values were calculated as follows (Laitano and Rosetti 2000):

$$s_{w,med} = \frac{\Sigma_i \int_{E^i_{cut}}^{E_{max}} \Phi^i_w(E)(L_\Delta(E)/\rho)^i_w dE + \Phi^i_w(E^i_{cut})\left(S_{el}(E^i_{cut})/\rho\right)^i_w E^i_{cut}}{\Sigma_i \int_{E^i_{cut}}^{E_{max}} \Phi^i_w(E)\,(L_\Delta(E)/\rho)^i_{med}\,dE + \Phi^i_w(E^i_{cut})\left(S_{el}(E^i_{cut})/\rho\right)^i_{med} E^i_{cut}}, \quad (1)$$

where $i = \{p, e, \alpha, \ldots\}$ are all the charged particles that contribute to the dose in the cavity; E^i_{cut} is the cut-off energy of the ith particle (for electrons, $E^e_{cut} \equiv \Delta$); $\Phi^i_w(E)$ is the distribution of the fluence of the ith particle in water with respect to the energy; and $(L_\Delta/\rho)^i_{med}$ and $(S_{el}/\rho)^i_{med}$ are the mass linear energy transfer and the mass electronic stopping power, respectively, of the ith particle in the medium. An upper limit for E^i_{cut} is typically defined as the mean energy of the ith particle with a sufficient residual range to cross the cavity. In this work, we set the size of the cavity equal to the typical height—in terms of mass-thickness—of a plane-parallel ionization chamber cavity, i.e. 2.5×10^{-4} g cm^{-2}. This setting leads to an upper limit for E_{cut} of 10 keV for electrons, 175 keV for protons, 250 keV for alphas, etc. For simplicity, we set $\Delta = 10$ keV for electrons and $E_{cut} = 100$ keV for protons and heavier particles.

The calculation of the $s_{w,med}$ values was performed 'off-line', i.e. we first calculated the distribution of the fluence with respect to the energy with Monte Carlo simulations and we afterwards calculated the $s_{w,med}$ values with equation (1). To overcome the potential deficiencies of an 'off-line' calculation, we used a dense ($\sim 10^3$) logarithmic energy binning. For the Monte Carlo simulations, we used GAMOS (Arce *et al* 2008)—a Monte Carlo simulation software framework based on the GEANT4 toolkit (Agostinelli *et al* 2003). As a reference beam, we simulated a zero-emittance beam (zero initial lateral spread and zero initial angular spread) with a zero initial energy spread impinging on a sufficiently large (15 cm radius) water phantom. We used the QGSP_BIC_EMY physics list (cf Cirrone *et al* (2009)), which combines the electromagnetic standard model for the electromagnetic processes, the binary cascade model for the hadronic inelastic processes, and an accurate tracking of electrons, hadrons and ions for dosimetry purposes. These physics settings have been proved to be suitable for the simulation of proton therapy beams (Zacharatou Jarlskog and Paganetti 2008). We set the production cuts for photons, electrons and positrons to 2.5 μm—to be consistent with our setting for the size of the cavity. We scored the (averaged) fluence of charged particles in a disc of water—perpendicular to the beam axis—of 0.1 mm thickness and 10 cm radius. We chose a sufficiently large radius to capture all the secondary charged particles scattered at large angles due to inelastic nuclear interactions. As mentioned before, we scored the fluence in a dense ($\sim 10^3$) set of logarithmic energy bins, from E_{cut} to E_{max}. We run as many particles as needed to achieve a standard statistical uncertainty in the final $s_{w,med}$ values lower than 0.1%. The total uncertainty, however, is much larger and it is mainly due to the uncertainty in the mean excitation energy values (I-values) of the different media. This point will be discussed later.

For the calculation of $s_{w,med}$ with equation (1), we first considered only the fluence of protons and electrons (Medin and Andreo 1997)—the influence of heavier particles is investigated later. For all materials except for water, we took the mass electronic stopping

powers (S_{el}/ρ) for protons and electrons directly from ICRU 49 (ICRU 1993) and ICRU 37 (ICRU 1984) respectively. When not tabulated, we calculated them with the Bragg additivity rule as suggested in ICRU 37—i.e. taking the I-values for the condensed phase of the elements in the compound. For water, however, we took the latest ICRU 73 (ICRU 2009) tentative value for I_w ($I_w = 78$ eV)—instead of the current ICRU 37 and ICRU 49 recommendation ($I_w = 75$ eV). Finally, the restricted linear electronic stopping powers (L_Δ) were calculated from S_{el} as suggested in ICRU 49.

We studied the effect of particles heavier than protons and track-ends on the calculation of the $s_{w,air}$. In this case, we scored all the charged particles that crossed the cavity. The calculation of the $s_{w,air}$ included alpha particles and all the ions with tabulated (S_{el}/ρ) values in ICRU 73 (ICRU 2005, ICRU 2009)—these were isotopes of lithium (^{6}Li, ^{7}Li, ^{8}Li), beryllium (^{6}Be, ^{7}Be, ^{9}Be, ^{10}Be), boron (^{8}B, ^{10}B, ^{11}B, ^{12}B, ^{13}B), carbon (^{10}C, ^{11}C, ^{12}C, ^{13}C, ^{14}C, ^{15}C), nitrogen (^{12}N, ^{13}N, ^{14}N, ^{15}N, ^{16}N, ^{17}N), oxygen (^{13}O, ^{14}O, ^{15}O, ^{16}O, ^{17}O, ^{18}O, ^{19}O), fluorine (^{17}F, ^{18}F, ^{19}F) and neon (^{20}Ne). We included them in equation (1) as follows: for alpha particles we calculated L_Δ; for heavier ions we assumed $L_\Delta \approx S_{el}$. This assumption is based on the fact that, for a given energy, the heavier the projectile, the lower the energy lost in a single collision with an electron in the medium, so the smallest the difference between L_Δ and S_{el}. In case this approximation was not sufficiently accurate, this would result in an overestimation of the contribution of these heavier ions to $s_{w,air}$.

The effect of the track-ends was simply assessed by calculating $s_{w,air}$ without the track-end term, i.e.

$$s_{w,air} = \frac{\Sigma_i \int_{E^i_{cut}}^{E_{max}} \Phi^i_w(E)\,(L_\Delta(E)/\rho)^i_w \,dE}{\Sigma_i \int_{E^i_{cut}}^{E_{max}} \Phi^i_w(E)\,(L_\Delta(E)/\rho)^i_{air} \,dE} \tag{2}$$

and comparing with the full equation (1). In this case, only the fluence of protons and electrons was taken into account.

We also investigated the effect of the initial energy spread of the beam on the $s_{w,air}$ values in depth. We investigated a Gaussian initial energy spread (σ_E/E) of 1%, which is representative of the values that can nowadays be achieved in modern proton therapy facilities—cf Clasie *et al* (2012).

Finally, we studied the $s_{w,med}$ values as a function of the radial distance (perpendicular to the beam direction). We took R_{80} as our definition of proton beam range—R_{80} is the depth at which the absorbed dose beyond the Bragg peak falls to 80% of its maximum value—and we modeled the lateral spread of the beam in depth due to multiple Coulomb scattering (MCS) with a Gaussian distribution with standard deviation σ_{MCS}. The calculation of σ_{MCS} was based on the generalized Fermi–Eyges multiple scattering theory (Safai *et al* 2008). We studied the effect of the radial distance at the depth of $R_{80}/2$, which is a depth with a broad halo of secondary protons for all energies (Pedroni *et al* 2005). In this case, the scoring volume was divided in concentric rings—with a width equal to $0.5\,\sigma_{MCS}$ at that depth.

3. Results and discussion

Figure 1(a) shows the Spencer–Attix $s_{w,air}$ values as a function of depth in water for different proton energies (30, 70, 150, 230 and 350 MeV). The depth in water is normalized to the range (R_{80}) of the proton beam. The numerical values are shown in table 1. As in Medin and Andreo (1997), we found that the peak-to-plateau ratio decreases with increasing energy—from 2.5% for 30 MeV beams to 1% for 350 MeV beams. This is due to the range straggling in water, which makes the proton energy spectrum at the Bragg peak region much broader for higher energies. Figure 1(b) shows a comparison of the Spencer–Attix $s_{w,air}$ values (for a 150 MeV

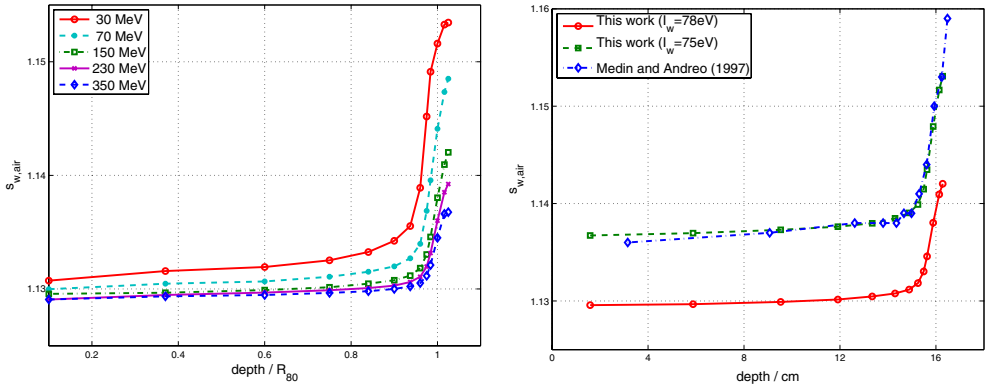

Figure 1. (a) Spencer–Attix $s_{w,air}$ values as a function of depth for proton beams of initial energy 30, 70, 150, 230 and 350 MeV. The values correspond to $I_w = 78$ eV. (b) Comparison of the $s_{w,air}$ values obtained in this work with the values published by Medin and Andreo (1997) for a 150 MeV proton beam.

Table 1. Spencer–Attix $s_{w,air}$ values as a function of depth for proton beams of initial energy 30, 70, 150, 230 and 350 MeV. The values correspond to $I_w = 78$ eV.

	Energy (MeV)				
Depth/R_{80}	30	70	150	230	350
0.100	1.131	1.130	1.130	1.129	1.129
0.370	1.132	1.130	1.130	1.129	1.129
0.600	1.132	1.131	1.130	1.130	1.129
0.750	1.133	1.131	1.130	1.130	1.130
0.840	1.133	1.132	1.130	1.130	1.130
0.900	1.134	1.132	1.131	1.130	1.130
0.937	1.136	1.133	1.131	1.131	1.130
0.960	1.139	1.134	1.132	1.131	1.131
0.975	1.145	1.137	1.133	1.132	1.131
0.984	1.149	1.140	1.135	1.133	1.132
1.000	1.152	1.144	1.138	1.136	1.135
1.016	1.153	1.147	1.141	1.139	1.137
1.025	1.153	1.149	1.142	1.139	1.137
R_{80} (cm)	0.90	4.11	15.87	31.92	66.62

beam) obtained in this work with GEANT4 and the values published by Medin and Andreo (1997) using PETRA. When using the same input data ($I_w = 75$ eV), an excellent agreement (differences $< 0.1\%$) was found between the two Monte Carlo codes. When using $I_w = 78$ eV, we found differences from 0.6% in the plateau region and up to 1% in the Bragg peak region. As already pointed out by other authors (cf Andreo (2009), Henkner *et al* (2009), Vatnitskiy *et al* (2010)), the uncertainty in the I-values is currently the largest source of uncertainty in the $s_{w,air}$ values. For relative dosimetry purposes however, the absolute $s_{w,air}$ values are not so critical; the only relevant quantities are the relative $s_{w,air}$ values along the beam range or, in other words, the peak-to-plateau ratio. Still, we found I_w has a noticeable effect on the peak-to-plateau ratio. For instance, for the 30 MeV beam, the peak-to-plateau ratio ranged from 2.8% for $I_w = 75$ eV to 2.0% when using $I_w = 78$ eV; for the 350 MeV beam, the peak-to-plateau

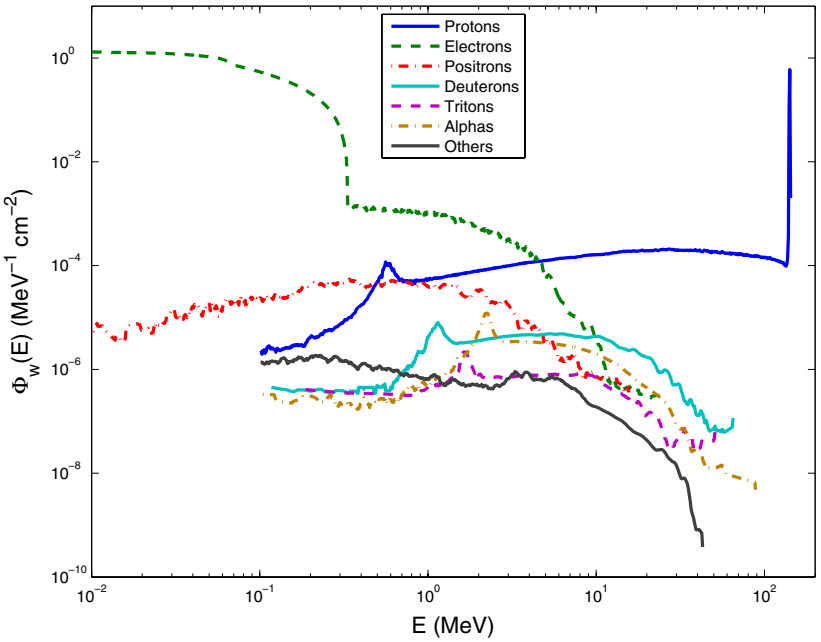

Figure 2. Distribution of the fluence of charged particles in water with respect to the energy per incident proton of initial energy 150 MeV at the depth of $R_{80}/10 = 1.6$ cm.

Table 2. Relative per cent contribution of the different charged particles to the absorbed dose to water and, within parenthesis, relative per cent contribution of the track-ends to the dose deposited by that particle. The plateau region is represented by the depth of $0.1\,R_{80}$; the peak region, by $0.984\,R_{80}$, which corresponds roughly to the depth of the maximum.

	30 MeV		150 MeV		350 MeV	
	Plateau	Peak	Plateau	Peak	Plateau	Peak
Protons	85.9 (0.0)	100 (0.2)	79.6 (0.0)	91.2 (0.0)	77.3 (0.0)	87.0 (0.0)
Electrons	13.6 (39)	0.0 (78)	19.2 (26)	8.6 (54)	20.7 (23)	12.5 (40)
Others	0.5 (0.1)	0.0 (3.0)	1.2 (0.5)	0.2 (0.3)	2.0 (0.4)	0.5 (0.4)

ratio ranged from 0.9% to 0.7%. The effect of the I-values on $s_{w,air}$ decreases with increasing energy. This is due to the fact that, the higher the energy of the projectile, the less relevant the I-value in the mass electronic stopping power of the projectile.

Figure 2 shows the distribution of the fluence of charged particles in water with respect to the energy generated by a proton beam of initial energy 150 MeV at the depth of $R_{80}/10 = 1.6$ cm. We found that the main contribution to the fluence comes from both protons and electrons; whereas the fluence of heavier particles is several orders of magnitude lower. Figure 2 also shows that the fluence of protons is clearly dominated by the primary protons and the fluence of electrons is clearly dominated by the proton-generated secondary electrons. The latter is shown by the drastic reduction of the electron fluence for $E > W_{max}$, where W_{max} is the largest possible energy loss of a proton in single collision with a free electron (cf ICRU 1993)—in this case, $W_{max} \sim 300$ keV. The major contribution of protons and electrons to the fluence does translate into a major contribution to the absorbed dose to water, as shown in table 2—where the relative contribution to D_w from the different charged particle species is

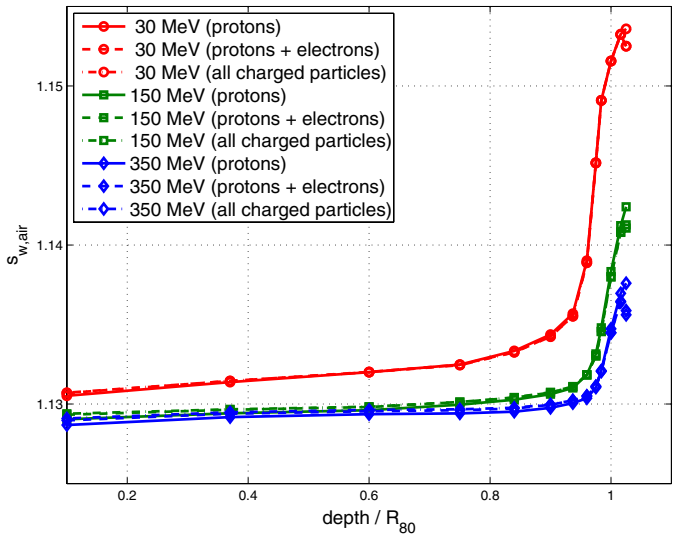

Figure 3. Spencer–Attix $s_{w,air}$ values as a function of depth for proton beams of initial energy 30, 150 and 350 MeV. The solid lines (——) include only protons, the dashed lines (- - - -) include protons and electrons, and the chain lines (— · —) include all charged particles.

shown. The significant contribution of the electrons to both the fluence and the absorbed dose to water, however, does not translate into a significant contribution to the $s_{w,air}$ values. Figure 3 shows the effect of including different charged particles (protons; both protons and electrons; and all charged particles) in the calculation of $s_{w,air}$ for different proton energies (30, 150 and 350 MeV). Systematic differences of the order of 0.1% were found when including electrons into equation (1), but no further significant differences were found when including the rest of particles heavier than protons. A similar behavior was found for the track-ends. Table 2 also shows the relative contribution of the track-ends to the dose deposited by each type of particle (within parenthesis). We found that, although electron track-ends can deposit up to 80% of the total dose deposited by the electrons, the minor role of the electrons in the $s_{w,air}$ values makes the contribution of these track-ends negligible. For protons and heavier particles, we found the contribution of the track-ends to D_w (and therefore to $s_{w,air}$) negligible—at least for the cut-off energy of $E_{cut} = 100\,\text{keV}$. Here, it is worth commenting on the need of including electrons in the calculation of the $s_{w,air}$ values. Medin and Andreo (1997) compared the Bragg–Gray $s_{w,air}$ values for protons with the Spencer–Attix $s_{w,air}$ values including both protons and electrons and they found differences of about 0.5%. In this work, we compared the Spencer–Attix $s_{w,air}$ values including protons and both protons and electrons and we found differences of only 0.1%. This leads to the conclusion that, when using L_Δ in the cavity integral—as in equation (1)—the inclusion of electrons in the calculation of $s_{w,air}$ is, to a very good approximation, not necessary.

Figure 4 shows the effect of the initial energy spread of the beam on the $s_{w,air}$ values as a function of depth in water for different proton energies (30, 150 and 350 MeV). A relative initial energy spread of 1% is compared to a zero initial energy spread. We found differences up to 0.5% in the Bragg peak region and no significant differences in the plateau. We also found the effect of the initial energy spread decreases with increasing energy. This is due to the fact that, at low energies, the total energy spread at the Bragg peak region is dominated by the initial energy spread of the beam whereas, at high energies, it is dominated by the range straggling in

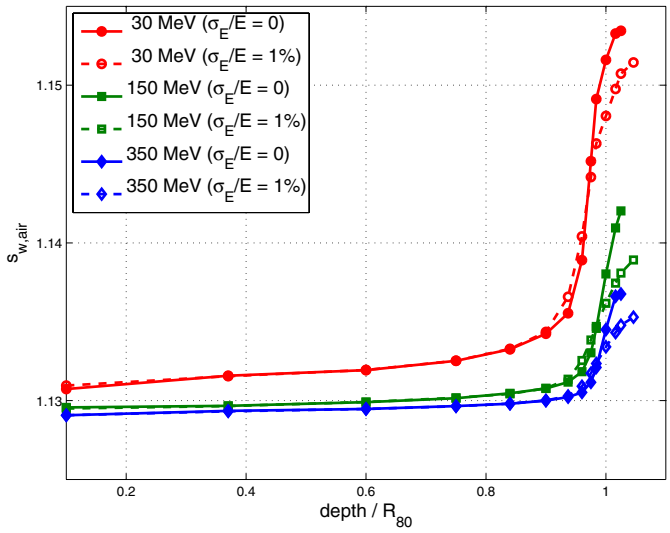

Figure 4. Spencer–Attix $s_{w,air}$ values as a function of depth for proton beams of initial energy 30, 150 and 350 MeV. The solid lines (——) show proton beams with initial $\sigma_E/E = 0$; the dashed lines (- - - -) show proton beams with initial $\sigma_E/E = 1\%$.

water. Furthermore, for the highest energy beams—meant for proton radiography (cf Depauw and Seco (2011))—one could argue that the initial energy spread of the beam has no effect on their relative dosimetry, since only the plateau region is used clinically. However, attention should be paid to low energy beams, where a narrow initial energy spread is technically more challenging—at least for cyclotron-based facilities—and its effect on the relative dosimetry should not be overlooked.

Figure 5 shows the $s_{w,med}$ values as a function of depth in water for different detection materials (air, EBT2, Gd_2O_2S:Tb, Si, LiF) and different proton energies (30, 150 and 350 MeV). The $s_{w,med}$ values are normalized to the entrance ($R_{80}/10$) value. Table 3 shows the absolute numerical values—for EBT2, gadolinium oxysulfide, Si and LiF—for proton beams of initial energy 30, 70, 150, 230 and 350 MeV. The numerical values for air are given in table 1. We found the $s_{w,med}$ values for air and EBT2 were quite constant (within 2.5%) along all depths. For lithium fluoride, the peak-to-plateau ratio went up to 5% (for 30 MeV). For silicon, we found peak-to-plateau ratios from 17% (for 30 MeV) down to 6% (for 350 MeV). Finally, for gadolinium oxysulfide, we found peak-to-plateau ratios from almost 60% (for 30 MeV) down to almost 20% (for 350 MeV). From these results, one could conclude that both air and EBT2 active layer seem to be appropriate detection materials for depth-dose measurements in water; LiF seems also to be acceptable given the typical uncertainties associated with thermoluminiscent dosimetry; while the use of silicon diodes should be discouraged—gadolinium oxysulfide is never used for this kind of measurements. Nevertheless, it is worth pointing out that: (i) the $s_{w,med}$ values assume that the detection material does not perturb the fluence in the medium, so a constant $s_{w,med}$ along all depths does not imply that the perturbation factor of the detector will also be constant at all depths—see, for instance, the measurement of depth-dose curves with a Farmer-type ionization chamber or with radiochromic films (Angellier *et al* 2011); and (ii) a constant $s_{w,med}$ and a constant detector perturbation factor at all depths means that the relationship between the absorbed dose to water and the absorbed dose to medium (D_{med}) is constant

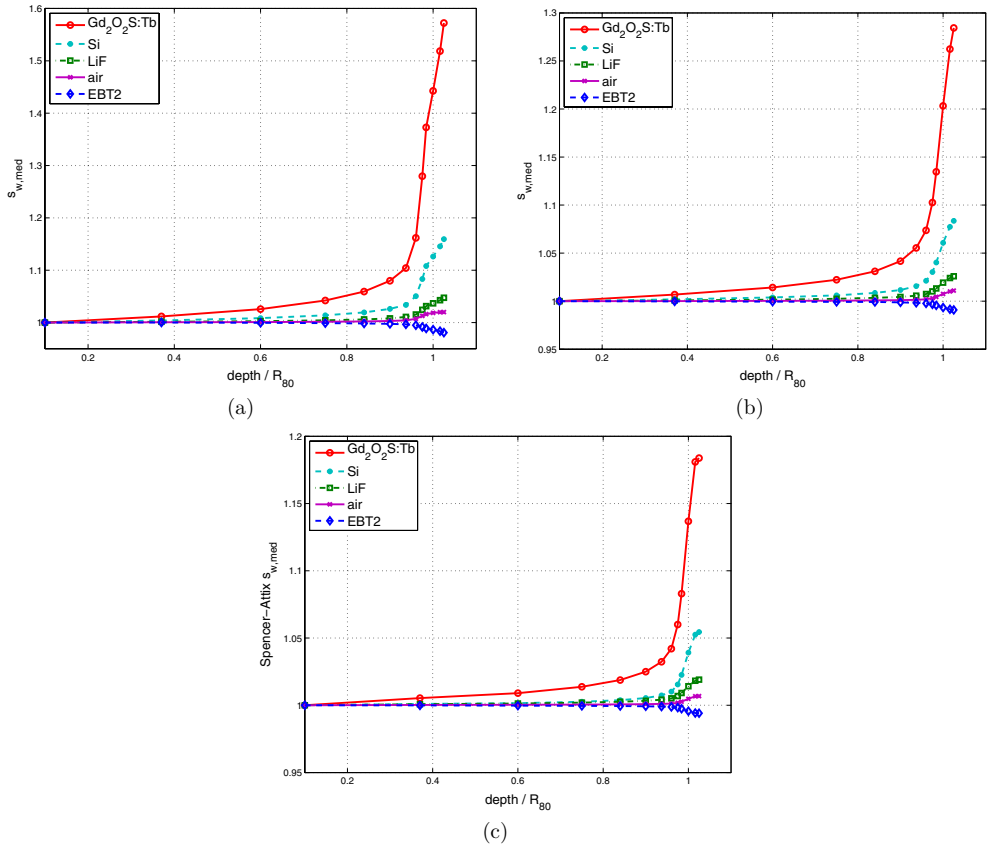

Figure 5. Spencer–Attix $s_{w,med}$ values as a function of depth for different detection materials (air, EBT2, Gd_2O_2S:Tb, Si and LiF) and different proton energies: (a) 30 MeV, (b) 150 MeV and (c) 350 MeV. The $s_{w,med}$ values are normalized to the entrance value.

at all depths, but this does not imply that the relationship between D_{med} and the detector reading/signal is also constant—see, for instance, the quenching effect in radiochromic films (Kirby *et al* 2010).

Figure 6 shows the $s_{w,med}$ values as a function of the radial distance (perpendicular to the beam axis) for different detection materials (air, EBT2, Gd_2O_2S:Tb, Si, LiF) and different proton energies (30, 150 and 350 MeV) at the depth of $R_{80}/2$. The $s_{w,med}$ values are normalized to the central axis value. The radial distance is normalized to the lateral spread of the beam due to MCS (σ_{MCS}) at that depth of $R_{80}/2$. We found that relative $s_{w,med}$ values start to differ from unity with increasing radial distance. This is due to the fact that, the larger the radial distance, the larger the relative contribution of secondary protons (with a much lower energy) to the total proton fluence, so the lower the mean energy of the spectrum. Similar results were reported by Andreo and Brahme (1981) for clinical electron beams. The region of clinical interest is the one where the absorbed dose to water has a non-negligible value—this is shown by the relative dose histogram plotted against the right axis in figure 6. Within this region, we found the $s_{w,med}$ values for air, EBT2 and LiF were constant along the radial distance (within 0.5% in the worst case scenario), and also for silicon (within 1%). For gadolinium oxysulfide, the tail-to-center ratio went from 1% (for 30 MeV) up to 3%

Table 3. Spencer–Attix $s_{w,med}$ values as a function of depth for different detection materials (EBT2, Gd_2O_2S:Tb, Si and LiF) and different proton energies (30, 70, 150, 230 and 350 MeV).

	Energy (MeV)					Energy (MeV)				
Depth/R_{80}	30	70	150	230	350	30	70	150	230	350
	EBT2 active-layer					Gadolinium oxysulfide				
0.100	0.997	0.998	0.999	0.999	0.999	1.999	1.932	1.896	1.885	1.880
0.370	0.997	0.999	0.999	0.999	0.999	2.022	1.949	1.909	1.898	1.890
0.600	0.997	0.998	0.999	0.999	0.999	2.050	1.968	1.923	1.908	1.897
0.750	0.996	0.998	0.998	0.999	0.999	2.083	1.992	1.938	1.919	1.906
0.840	0.995	0.997	0.998	0.998	0.999	2.118	2.018	1.954	1.931	1.915
0.900	0.995	0.997	0.998	0.998	0.999	2.159	2.051	1.974	1.947	1.927
0.937	0.994	0.996	0.997	0.998	0.998	2.207	2.089	2.001	1.966	1.941
0.960	0.992	0.995	0.997	0.998	0.998	2.323	2.142	2.035	1.992	1.959
0.975	0.989	0.993	0.996	0.997	0.997	2.558	2.245	2.090	2.036	1.993
0.984	0.986	0.992	0.995	0.996	0.997	2.745	2.342	2.151	2.087	2.036
1.000	0.984	0.989	0.992	0.994	0.995	2.884	2.520	2.281	2.201	2.137
1.016	0.981	0.987	0.991	0.992	0.993	3.036	2.664	2.393	2.297	2.220
1.025	0.978	0.986	0.990	0.992	0.993	2.143	2.726	2.435	2.321	2.226
	Silicon					Lithium fluoride				
0.100	1.302	1.289	1.282	1.281	1.281	1.235	1.231	1.229	1.227	1.227
0.370	1.307	1.292	1.285	1.283	1.283	1.237	1.233	1.229	1.228	1.228
0.600	1.313	1.296	1.287	1.285	1.283	1.238	1.234	1.230	1.229	1.228
0.750	1.320	1.301	1.290	1.287	1.285	1.241	1.235	1.231	1.230	1.229
0.840	1.327	1.306	1.293	1.289	1.286	1.243	1.237	1.233	1.231	1.230
0.900	1.336	1.313	1.297	1.292	1.288	1.245	1.239	1.234	1.232	1.231
0.937	1.345	1.321	1.302	1.296	1.291	1.249	1.241	1.236	1.233	1.232
0.960	1.367	1.332	1.310	1.301	1.294	1.254	1.244	1.238	1.235	1.233
0.975	1.410	1.353	1.321	1.310	1.301	1.265	1.250	1.241	1.238	1.235
0.984	1.442	1.372	1.334	1.321	1.310	1.274	1.256	1.245	1.241	1.238
1.000	1.466	1.404	1.360	1.344	1.332	1.281	1.264	1.252	1.248	1.244
1.016	1.491	1.429	1.382	1.364	1.349	1.288	1.271	1.258	1.253	1.249
1.025	1.510	1.439	1.390	1.369	1.351	1.294	1.274	1.260	1.255	1.250

(for 150 and 350 MeV). From these results, one could argue that scintillating screens might not be the most suitable detectors for lateral dose profiles measurements in depth. However, this kind of detectors are typically used to measure the lateral dose profiles in air. In this case, the number of secondary protons scattered at large radial distances is much smaller and, hence, the relative stopping-power ratios along the radial distance are likely to remain constant.

Finally, it is of interest to comment that, although updated $s_{w,air}$ values for reference ionization chamber dosimetry of proton beams were included in table 1, calculations of beam quality correction factors (k_Q) were not included in this work. One reason for that is the lack of accurate perturbation correction factors for the most widely used types of ionization chambers—where only approximate analytical calculations (cf Palmans and Verhaegen (1998), Palmans (2006)) were available so far. Recent work by Palmans (2011a) has summarized the current status of ionization chamber perturbation factors, describing a model that estimates the electron spectrum produced by the incident protons numerically, followed by an independent electron Monte Carlo simulation to determine the 'perturbed electron spectrum' created by the presence of a simplified cylindrical ionization chamber in water. In general, the perturbation factors for graphite-walled ionization chambers are estimated to be close to unity, but this

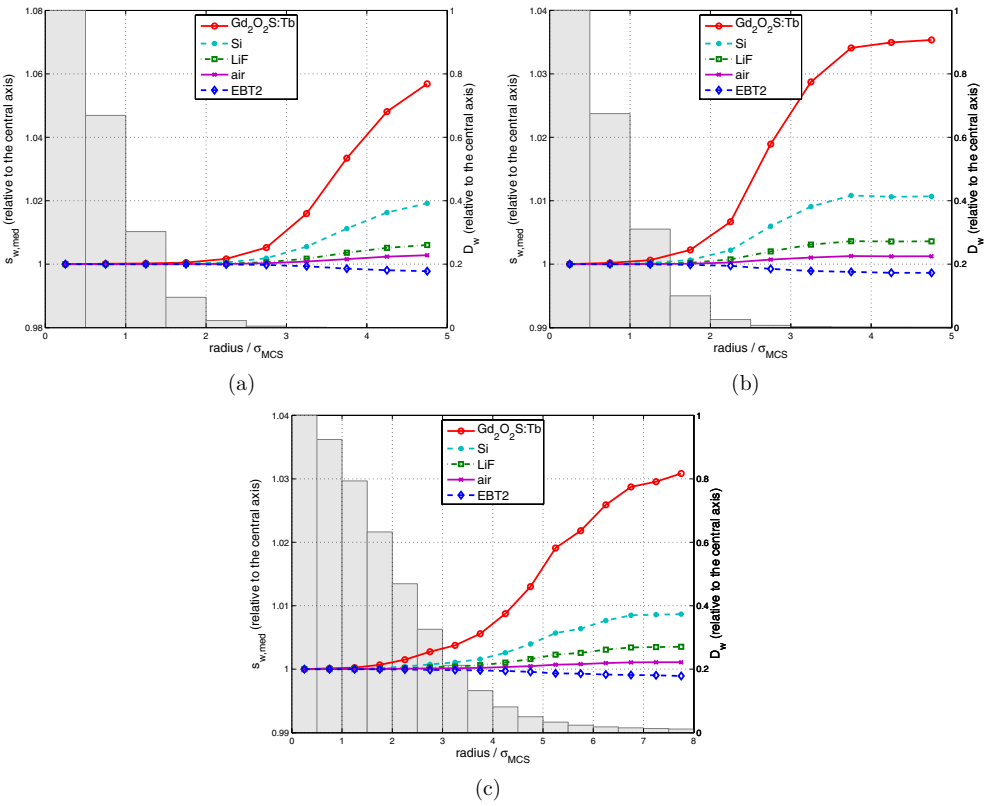

Figure 6. Spencer–Attix $s_{w,med}$ values (plotted against the left axis) and histogram of the absorbed dose to water (plotted against the right axis) as a function of radial distance for different detection materials (air, EBT2, Gd_2O_2S:Tb, Si and LiF) and different proton energies: (a) 30 MeV, (b) 150 MeV and (c) 350 MeV. Both $s_{w,med}$ values and dose values are normalized to the central axis value.

has not yet been confirmed with consistent and detailed Monte Carlo calculations in proton beams in a similar way to those done for electron (cf Sempau *et al* (2004)) and photon beams (cf Panettieri *et al* (2008), Wulff *et al* (2008)). More significant is the current uncertainty in the dosimetry of ^{60}Co beams—which continue to be the reference beam quality for most therapeutic beams. Beam quality correction factors include data from ^{60}Co, either as a normalizing calibration factor ($N_{D,w,^{60}Co}$) in an experimental k_Q, or as the product of the $s_{w,air}$ and the chamber perturbation correction factors, $(s_{w,air}\ p)_{^{60}Co}$, in the denominator of a calculated k_Q. Even though recent data has considerably decreased the uncertainty of some perturbation factors—placing almost at a comparable level the use of cylindrical and plane-parallel ionization chambers—new concerns have been raised (Benmakhlouf and Andreo 2011). For ^{60}Co and all types of charged particles that use ^{60}Co as a reference quality (i.e. electrons, protons and heavier ions), the new available perturbation factors data would yield a change in absorbed dose of up to about 1.5%, representing a considerable discrepancy with current proton calorimetry (cf Palmans (2011b)). In the case of megavoltage photon beams, a partial cancellation of potential systematic errors occurs, yielding smaller differences. In addition, all this new data has been determined for $I_w = 75$ eV. It seems therefore reasonable to postpone the calculation of k_Q values until the ^{60}Co issue is clarified and updated data for $(s_{w,air}\ p)_{^{60}Co}$ becomes available.

4. Conclusions

In this work, we calculated the Spencer–Attix water/medium stopping-power ratios for the dosimetry of clinical proton pencil beams. From the results obtained for $s_{w,air}$, we found that protons are—to a very good approximation—the only particles that need to be included in the calculation of the stopping-power ratios. The inclusion of electrons systematically increases the $s_{w,air}$ values by 0.1%, whereas the inclusion of track-ends and particles heavier than protons does not have any effect on the $s_{w,air}$ values. In contradistinction, the choice of the I-values has a large effect on the $s_{w,air}$ values—not only on the absolute values necessary for reference dosimetry, but also on the relative values (peak-to-plateau ratio) necessary for relative dosimetry. A difference of 3 eV in I_w results in a difference in the $s_{w,air}$ values of approximately 0.6% in the plateau region and in an additional difference from 0.2% (350 MeV) to 0.7% (30 MeV) in the Bragg peak region. Clearly, the uncertainty in the I-values is nowadays the largest source of uncertainty in the stopping-power ratios. Despite this uncertainty, a correction is still needed for depth-dose measurements to compensate for the different $s_{w,med}$ values between the plateau and the Bragg peak region. The most suitable detection materials for depth-dose measurements in water were found to be air and EBT2 active layer. Based on the calculations made with $I_w = 78$ eV, a correction from roughly 1% (350 MeV) to 2.5% (30 MeV) should be used in the Bragg peak region for these two detection materials. The corrections needed for LiF—from roughly 2% (350 MeV) to 5% (30 MeV)—are also acceptable given the typical uncertainties associated with thermoluminiscent dosimetry. The use of silicon and gadolinium oxysulfide for depth-dose measurements in water should be discouraged. In addition, the initial energy spread of the beam has little effect (<0.5%) on the $s_{w,air}$ values in depth. We therefore believe that, given the overall uncertainties, a single (already energy-dependent and depth-dependent) correction could be used, irrespective of the initial energy spread of the beam. As for in-depth lateral dose profiles and field-specific dose distributions, all the studied detection materials—except for gadolinium oxysulfide—would be appropriate for these kinds of measurements. In the case of gadolinium oxysulfide, we believe that it could still be used for lateral dose profiles and field-specific dose distribution measurements in air. Overall, we found that proton radiography beams are more forgiving to relative dosimetry subtleties whereas very low energy beams—such as 30 MeV beams—are more demanding, so special attention should be paid to their relative dosimetry.

Acknowledgments

The authors would like to thank Pedro Arce for his support with GAMOS. CG would also like to thank Sairos Safai for the enriching discussions about the physics of proton therapy beams, and Dirk Boye for his programming tips. JS is grateful to the Spanish Ministerio de Economía y Competitividad (project no. FIS2012-38480), to the Spanish Ministerio de Ciencia e Innovación (project no. FPA2009-14091-C02-01) and to the Spanish Networking Research Center CIBER-BBN.

References

Agostinelli S *et al* 2003 Geant4—a simulation toolkit *Nucl. Instrum. Methods Phys. Res.* A **506** 250–303

Albertini F, Casiraghi M, Lorentini S, Rombi B and Lomax A J 2011 Experimental verification of IMPT treatment plans in an anthropomorphic phantom in the presence of delivery uncertainties *Phys. Med. Biol.* **56** 4415–31

Andreo P 2009 On the clinical spatial resolution achievable with protons and heavier charged particle radiotherapy beams *Phys. Med. Biol.* **54** N205–15

Andreo P and Brahme A 1981 Mean energy in electron beams *Med. Phys.* **8** 682–7

Andreo P, Burns D T, Hohlfeld K, Huq M S, Kanai T, Laitano F, Smyth V and Vynckier S 2000 Absorbed dose determination in external beam radiotherapy: an international code of practice for dosimetry based on standards of absorbed dose to water *IAEA Technical Report Series No. 398* (Vienna: IAEA)

Angellier G, Gautier M and Hérault J 2011 Radiochromic EBT2 film dosimetry for low-energy protontherapy *Med. Phys.* **38** 6171–7

Arce P, Rato P, Canadas M and Lagares J I 2008 GAMOS: a GEANT4-based easy and flexible framework for nuclear medicine applications *IEEE Nuclear Science Symp. Conf. Record* pp 3162–8

Ashland 2011 Gafchromic EBT2 (available at: http://gafchromic.com)

Benmakhlouf H and Andreo P 2011 Ten years after: impact of recent research in photon and electron beam dosimetry on the IAEA TRS-398 code of practice *Proc. Int. Conf. on Standards, Applications and Quality Assurance in Medical Radiation Dosimetry (Vienna, 2010)* (Vienna: IAEA) pp 139–52

Boon S N, van Luijk P, Böhringer T, Coray A, Lomax A, Pedroni E, Schaffner B and Schippers J M 2000 Performance of a fluorescent screen and CCD camera as a two-dimensional dosimetry system for dynamic treatment techniques *Med. Phys.* **27** 2198–208

Cirrone G A P *et al* 2009 Hadrontherapy: an open source, Geant4-based application form proton–ion therapy studies *IEEE Nuclear Science Symp. Conf. Record* pp 4186–9

Clasie B, Depauw N, Fransen M, Gomà C, Panahandeh H R, Seco J, Flanz J B and Kooy H M 2012 Golden beam data for proton pencil-beam scanning *Phys. Med. Biol.* **57** 1147–58

Depauw N and Seco J 2011 Sensitivity study of proton radiography and comparison with kV and MV x-ray imaging using GEANT4 Monte Carlo simulations *Phys. Med. Biol.* **56** 2407–21

Ferrari A, Sala P R, Fassò A and Ranft J 2005 FLUKA: a multi-particle transport code *Technical Report* CERN-2005-010, INFN TC_05/11, SLAC-R-773

Gillin M T *et al* 2010 Commissioning of the discrete spot scanning proton beam delivery system at the University of Texas M.D. Anderson Cancer Center, Proton Therapy Center, Houston *Med. Phys.* **37** 154–63

Grassberger C and Paganetti H 2011 Elevated LET components in clinical proton beams *Phys. Med. Biol.* **56** 6677–91

Henkner K, Bassler N, Sobolevsky N and Jäckel O 2009 Monte Carlo simulations on the water-to-air stopping power ratio for carbon ion dosimetry *Med. Phys.* **36** 1230–5

ICRU 1984 Stopping Powers for Electrons and Positrons *ICRU Report No. 37* (Bethesda, MD: ICRU)

ICRU 1993 Stopping Powers and Ranges for Protons and Alpha Particles *ICRU Report No. 49* (Bethesda, MD: ICRU)

ICRU 2005 Stopping of Ions Heavier than Helium *ICRU Report No. 73* (Bethesda, MD: ICRU)

ICRU 2007 Prescribing, Reporting and Recording Proton-beam Therapy *ICRU Report No. 78* (Bethesda, MD: ICRU)

ICRU 2009 Errata and Addenda for ICRU Report 73: Stopping of Ions Heavier than Helium *ICRU Report No. 73* (Bethesda, MD: ICRU)

Karger C P, Jäckel O, Palmans H and Kanai T 2010 Dosimetry for ion beam radiotherapy *Phys. Med. Biol.* **55** R193–234

Kirby D, Green S, Palmans H, Hugtenburg R, Wojnecki C and Parker D 2010 LET dependence of GafChromic films and an ion chamber in low-energy proton dosimetry *Phys. Med. Biol.* **55** 417–33

Laitano R F and Rossetti M 2000 Proton stopping powers averaged over beam energy spectra *Phys. Med. Biol.* **45** 3025–43

Medin J and Andreo P 1997 Monte Carlo calculated stopping-power ratios, water/air, for clinical proton dosimetry (50–250 MeV) *Phys. Med. Biol.* **42** 89–105

Nahum A 1978 Water/air mass stopping power ratios for megavoltage photon and electron beams *Phys. Med. Biol.* **23** 24–38

Palmans H 2006 Perturbation factors for cylindrical ionization chambers in proton beams. Part I: corrections for gradients *Phys. Med. Biol.* **51** 3483–501

Palmans H 2011a Secondary electron perturbations in Farmer type ion chambers for clinical proton beams *Proc. Int. Symp. on Standards, Applications and Quality Assurance in Medical Radiation Dosimetry (Vienna, 2010)* (Vienna: IAEA) pp 309–17

Palmans H 2011b Dosimetry *Proton Therapy Physics* ed H Paganetti (Boca Raton, FL: CRC Press) pp 191–219

Palmans H and Verhaegen F 1998 Monte Carlo study of fluence perturbation effects on cavity dose response in clinical proton beams *Phys. Med. Biol.* **43** 65–89

Panettieri V, Sempau J and Andreo P 2008 Chamber-quality factors in 60Co for three plane-parallel chambers for the dosimetry of electrons, protons and heavier charged particles: PENELOPE Monte Carlo simulations *Phys. Med. Biol.* **53** 5917–26

Pedroni E, Scheib S, Böhringer T, Coray A, Grossmann M, Lin S and Lomax A 2005 Experimental characterization and physical modelling of the dose distribution of scanned proton pencil beams *Phys. Med. Biol.* **50** 541–61

Safai S, Bortfeld T and Engelsman M 2008 Comparison between the lateral penumbra of a collimated double-scattered beam and uncollimated scanning beam in proton radiotherapy *Phys. Med. Biol.* **53** 1729–50

Schwaab J, Brons S, Fleres J and Parodi K 2011 Experimental characterization of lateral profiles of scanned proton and carbon ion pencil beams for improved beam models in ion therapy treatment planning *Phys. Med. Biol.* **56** 7813–27

Sempau J, Andreo P, Aldana J, Mazurier J and Salvat F 2004 Electron beam quality correction factors for plane-parallel ionization chambers: Monte Carlo calculations using the PENELOPE system *Phys. Med. Biol.* **49** 4427–44

Vatnitskiy S, Andreo P and Jones D T L 2010 Recent advances in dosimetry in reference conditions for proton and light-ion beams *Proc. Int. Symp. on Standards, Applications and Quality Assurance in Medical Radiation Dosimetry (Vienna, 2010)* (Vienna: IAEA) pp 357–66

Wulff J, Heverhagen J T and Zink K 2008 Monte-Carlo-based perturbation and beam quality correction factors for thimble ionization chambers in high-energy photon beams *Phys. Med. Biol.* **53** 2823–36

Zacharatou Jarlskog C and Paganetti H 2008 Physics settings for using the GEANT4 toolkit in proton therapy *IEEE Trans. Nucl. Sci.* **55** 1018–25